論文 / 著書情報
Article / Book Information

Title	Does Thin-Walled Metal Pipe Insertion Increase the Bending Strength of 3D Printed Parts?
Authors	Kurumi Osawa, Gen Endo
Citation	Proceedings of the 2024 IEEE/SICE International Symposium on System Integration, , , pp. 585-591
Pub. date	2024, 1
Copyright	(c) 2024 IEEE. Personal use of this material is permitted. Permission from IEEE must be obtained for all other uses, in any current or future media, including reprinting/republishing this material for advertising or promotional purposes, creating new collective works, for resale or redistribution to servers or lists, or reuse of any copyrighted component of this work in other works.
DOI	http://dx.doi.org/10.1109/SII58957.2024.10417167
Note	This file is author (final) version.

Does Thin-Walled Metal Pipe Insertion Increase the Bending Strength of 3D Printed Parts?

Kurumi Osawa[1] and Gen Endo[1]

***Abstract*— Resin 3D printing is a promising modeling method for Agile development, however its material strength is lower than that of metal parts. We hypothesized that embedding a thin-walled metal pipe in a 3D printed beam would increase the strength of the part while keeping it lightweight. This paper aims to verify the effectiveness of this method. To test our hypothesis, specimens of potassium titanate fiber-reinforced material POTICON and ABS were fabricated, and conducted three-point bending tests. As a result, POTICON specimens embedded with stainless steel pipes showed a strength 0.7 to 1.4 times that of the solid specimens, while ABS specimens showed a strength 1.1 to 2.0 times greater than the solid specimens. These values were small compared to our flexural rigidity calculations, and we concluded that embedding a pipe did not significantly increase the strength.**

I. INTRODUCTION

In recent years, 3D printers have become increasingly popular. They are available in various types, including fused deposition modeling (FDM), stereolithography (SLA), material jetting, and binder jetting, which mainly use resin. There are also selective laser melting (SLM), selective laser sintering (SLS), electron beam melting (EBM), and others that use metallic materials [1] [2]. FDM, also known as fused filament fabrication (FFF), is a method of fabrication in which thermoplastic resin filament material is melted by heat and extruded from a nozzle. It is the most widely used method because it is cost-effective and easy to obtain materials. This type of printer is also said to be an environmentally safe desktop prototyping facility because it produces only a small amount of waste [3].

The widespread use of FFF 3D printers has made it possible to fabricate parts faster and lighter than machining metal. Previous research have developed speed reducers and robots using resin parts fabricated by 3D printers [4]–[9]. However, resin has significantly lower strength than metal, making it difficult to use in situations where large loads are applied. Therefore, methods to increase the strength of resin parts have been investigated, such as reinforcement by continuous carbon fiber [10] [11], reinforcement by optimizing materials [12], and reinforcement of structurally weak parts by varying the internal density [13]. Among these methods, the method of inserting continuous carbon fiber is easiest to attempt because 3D printers that can achieve this are commercially available [14], however it is difficult to freely allocate the carbon fiber due to the limitations of the slicer software. In addition, many previous studies have experimentally evaluated the mechanical properties of resins produced by 3D printers. With lessons learned from these studies, it is possible to build parts using stronger resins and printing parameters (number of layers, printing speed, nozzle temperature, etc.) that can improve the strength of the part [15]–[17]. However, there are limits to the types of resins and printing parameters covered above, and even if the most suitable ones are employed, it is not always possible to achieve sufficient strength to meet the required specifications. Therefore, we propose a new method of reinforcing resin by embedding a thin-walled metal pipe into a resin beam fabricated by a 3D printer. We hypothesized that the metal would support some of the load applied to the resin, thereby increasing the strength of the part. The purpose of this paper is to verify the effectiveness of this method and to experimentally measure the strength by conducting a three-point bending test.

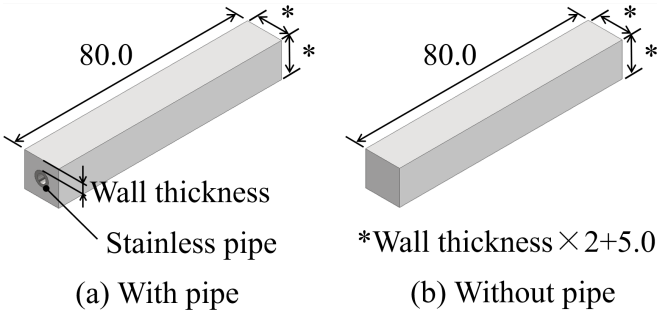

Fig. 1. Specimen

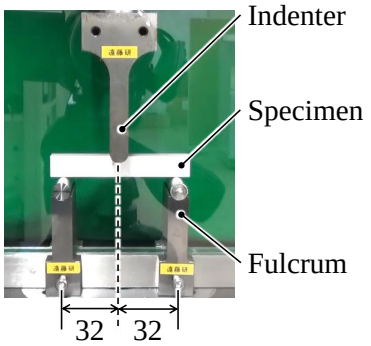

Fig. 2. The actual condition of the experiment

II. EXPERIMENTAL SETUP

A. Test Procedure

To verify the proposed method, resin specimens with embedded metal pipes (Fig. 1(a)) and solid resin specimens

[1]All authors are with the Department of Mechanical Engineering, Tokyo Institute of Technology, 2-12-1 Ookayama, Meguroku, Tokyo 152-8552, Japan osawa.k.af, endo.g.aa@m.titech.ac.jp

TABLE I

MATERIAL PROPERTY

Material	POTICON	ABS
Tensile strength (MPa)	100	32.60
Bending strength (MPa)	167	54.00
Flexural modulus (GPa)	6.3	1.85
Specific density (g/cm^3)	1.27	1.179
Heat deflection temperature (°C)	120	106.40

without embedded metal pipes (Fig. 1(b)) were prepared, and three-point bending tests were conducted using an Autograph (Shimadzu Corporation, AG-1 and AGX-20kNVD). Referring to ISO 178:2010, the length of each specimen was set to 80 mm, and the distance between the fulcrums of the bending test was set to 64 mm, the test speed to 2 mm/min, and the indenter radius to 5 mm. The indenter was adjusted so that it was positioned in the center of the specimen, and the displacement and load were measured until the specimen fractured. The test is shown in Fig. 2. Since the dimensions of 3D printed parts may slightly differ from those on CAD, the actual dimensions were measured and the CAD dimensions were fine-tuned to achieve the dimensions shown in Fig. 1.

B. Materials

The 3D printer used was a Raise3D Pro2, which is FFF type. Two types of resin were used for the specimens: a potassium titanate fiber-reinforced material called POTICON by Otsuka Chemical Co., Ltd. [18], and Z-ULTRAT which is an ABS-based material by Zortrax. The physical properties of the resins are shown in TABLE I [19] [20]. To the best of our knowledge, POTICON is the strongest short fiber-reinforced filament material for FFF type 3D printers. The slicer software used was ideaMaker, which is dedicated to Raise3D. The metal pipe used was SUS304 grade with an outer diameter of $\phi 5$ and an inner diameter of $\phi 3$. The specimen with the embedded pipe was fabricated by making a specimen with a hole of $\phi 5.3$ without support using a 3D printer, and then pressing the pipe directly into the specimen. In the case of adhesion, an adhesive (Cemedine Co., Ltd., Super X No. 8008) with acrylic modified silicone resin as the main component was applied to the pipe and then pressed into the specimen.

C. Printing Conditions

The infill density of the resin was set to 100%. Since the purpose of the test was to increase the strength of the resin, infill density below 100%, which would clearly reduce the strength, were not included. On the other hand, the lamination direction, wall thickness, and whether or not the pipe is adhered, which may have a correlation with strength, were verified in the tests. The lamination directions are shown in Fig. 3, the wall thickness is the dimension shown in Fig. 1 and is 2.4 mm and 3.6 mm, and the pipe adhesion is compared under three conditions, including one without embedded pipes. As shown in Fig. 4, straight line infill with one shell was used for lamination in the Z direction, and concentric circle infill with one shell was used

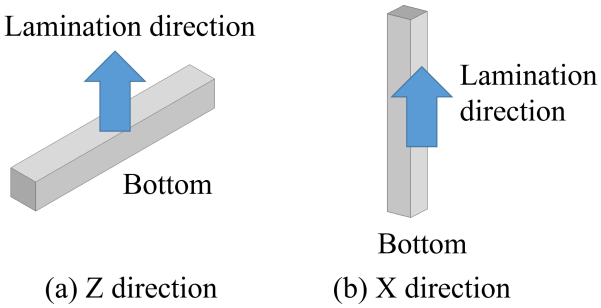

Fig. 3. Lamination direction

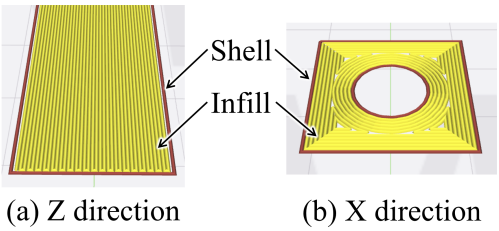

Fig. 4. Infill pattern

TABLE II

SPECIMEN PROPERTIES

Number	Lamination	Wall (mm)	Pipe
A	Z	3.6	Insert
B	Z	3.6	Adhere
C	Z	3.6	None
D	X	3.6	Insert
E	X	3.6	Adhere
F	X	3.6	None
G	Z	2.4	Insert
H	Z	2.4	Adhere
I	Z	2.4	None

for lamination in the X direction. This is because a triangular infill pattern tends to create a gap inside the specimen, which increases the possibility of internal fractures. The specimens fabricated to verify the above conditions are summarized in TABLE II; three specimens were fabricated and tested for each condition. Since the nozzle diameter and extrusion width were set to 0.4 mm and 0.3 mm, respectively, when the specimens were fabricated, the wall thicknesses were set to 2.4 mm and 3.6 mm, which are multiples of these values. The dimensions of the specimens without embedded pipes were matched to those of the specimens with embedded pipes for comparison.

D. Evaluation Method

We obtained load and displacement data from a 3-point bending test. Using these values, stress σ and strain ε were evaluated.

First, area moment of inertia is calculated. For the cross section shown in Fig. 5, the area moment of inertia is four times that in the region represented by $y \geq 0$ and $z \geq 0$. To simplify the calculation, the equivalent area moment of inertia I (mm^4) is calculated assuming that all materials are resin. The calculation can be done as follows.

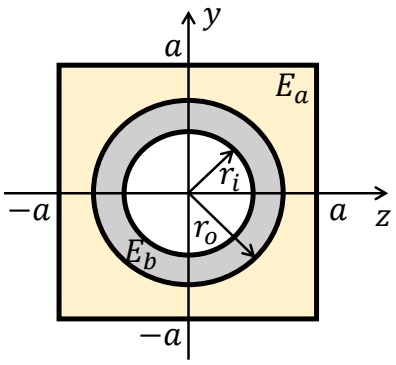

Fig. 5. Cross section model

$$I = 4\left[\int_0^{r_o}\left\{\frac{E_b}{E_a}\sqrt{r_o^2-y^2}+(a-\sqrt{r_o^2-y^2})\right\}y^2dy + \int_{r_o}^{a}y^2ady - \int_0^{r_i}\frac{E_b}{E_a}\sqrt{r_i^2-y^2}y^2dy\right] = \frac{r_o^3(16a-3\pi r_o)}{12}+\frac{4a(a^3-r_o^3)}{3}+\frac{\pi E_b(r_o^4-r_i^4)}{4E_a} \quad (1)$$

where E_a (GPa) is the flexural modulus of the resin, and E_b (GPa) is that of the pipe. The process of deriving the equation is described in the Appendix.

Since I is the equivalent area moment of inertia of the resin, the stress σ (GPa) and strain ε at the center of the beam and $y = a$ are calculated as follows.

$$\sigma = \frac{E_a}{\rho}y = \frac{M}{I}y = \frac{FLa}{4I} \quad (2)$$

$$\varepsilon = \frac{1}{\rho}y = \frac{\sigma}{E_a} = \frac{FLa}{4I}\times\frac{48vI}{FL^3} = \frac{12va}{L^2} \quad (3)$$

where F (kN) is the load, v (mm) is the displacement, ρ (mm) is the radius of curvature of displacement v, M (Nm) the moment applied to the center of the beam and L (mm) is the distance between the fulcrum points.

Since embedding the metal pipe in the resin increases the mass of the specimen, the specific strength is also evaluated. The specific strength (Nm/g) is calculated using the following equation.

$$\text{Specific strength} = \frac{\sigma_{max}}{\text{Density}} \quad (4)$$

where σ_{max} (GPa) is the maximum stress. the density of the specimen ($\mathrm{g/mm^3}$) can be calculated by measuring the mass (g) and volume ($\mathrm{mm^3}$) of each specimen.

III. FLEXURAL RIGIDITY CALCULATION

The specimens with and without pipes are quantitatively compared. First, a solid cylinder of resin and a stainless steel pipe were compared to confirm the greater strength of the pipe. The flexural rigidity of the solid resin cylinder EI_{rod} ($\mathrm{Nm^2}$) and that of the stainless steel pipe EI_{pipe} ($\mathrm{Nm^2}$) can be expressed as follows.

TABLE III
CALCULATED FLEXURAL RIGIDITY OF ROD AND PIPE

Shape	Material	Flexural rigidity ($\mathrm{Nm^2}$)
Cylinder	POTICON	0.19
Cylinder	ABS	0.056
Pipe	SUS304	5.2

TABLE IV
CALCULATED FLEXURAL RIGIDITY OF SPECIMEN

Material	Wall (mm)	Pipe	Flexural rigidity ($\mathrm{Nm^2}$)
POTICON	3.6	√	16.6
POTICON	3.6		11.6
POTICON	2.4	√	9.8
POTICON	2.4		4.8
ABS	3.6	√	8.5
ABS	3.6		3.4
ABS	2.4	√	6.5
ABS	2.4		1.4

$$EI_{rod} = \frac{E_a}{1000}\frac{\pi D^4}{64} \quad (5)$$

$$EI_{pipe} = \frac{E_b}{1000}\frac{\pi(D^4-d^4)}{64} \quad (6)$$

where D (mm) is the outer diameter of the pipe, d (mm) is the inner diameter of the pipe.

The flexural moduli of the resins are shown in TABLE I, and the modulus of the SUS304 used for this pipe is $E_b = 193$ GPa. Therefore, the flexural rigidity can be calculated as shown in TABLE III. These values show that, the flexural rigidity of the stainless steel pipe is about 27 times greater than that of POTICON and about 93 times greater than that of ABS, which is a significantly large value.

On the other hand, the flexural rigidity of the specimen $EI_{specimen}$ ($\mathrm{Nm^2}$) can be expressed as follows.

$$EI_{specimen} = \frac{E_aI}{1000} \quad (7)$$

In the case of no pipe, (1) holds if $D = 0, d = 0$. Therefore, without considering the lamination direction, the flexural rigidity can be calculated as in TABLE IV. This indicates that the flexural rigidity with pipe is approximately 1.4 to 4.6 times greater than without pipe.

Based on the above calculations, we expect that the flexural rigidity and strength would be different, but that the addition of the pipe would increase the strength.

IV. TEST RESULTS

A. Stress-Strain Diagram

The results for POTICON are shown in Fig. 6 and the results for ABS are shown in Fig. 7. The avg. shown in Fig. 6 and 7 represents the average value of the maximum stress at the moment the specimen fractured in each of the three tests. In the case of ABS D in Fig. 6, the maximum stress was reached after the resin part of the specimen fractured due to the presence of the pipe, but the maximum stress was

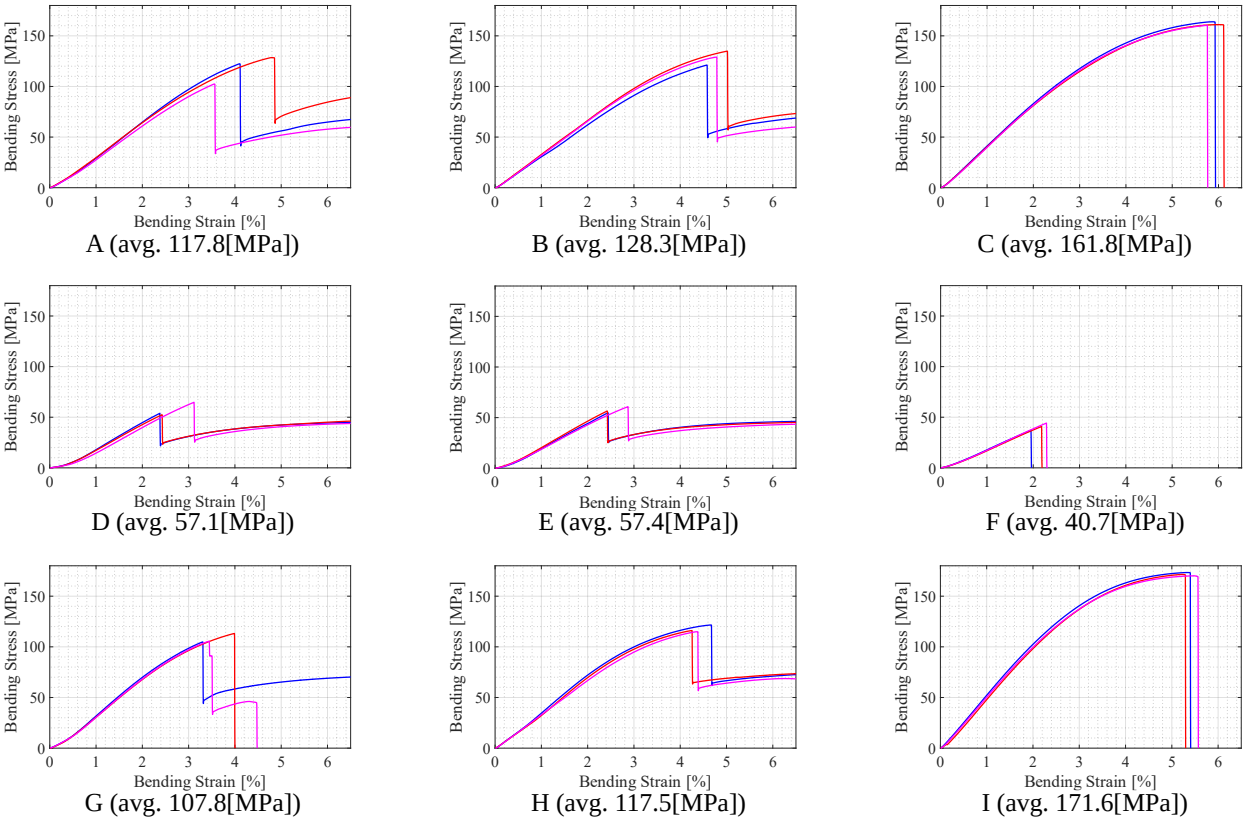

Fig. 6. Experimental results of POTICON

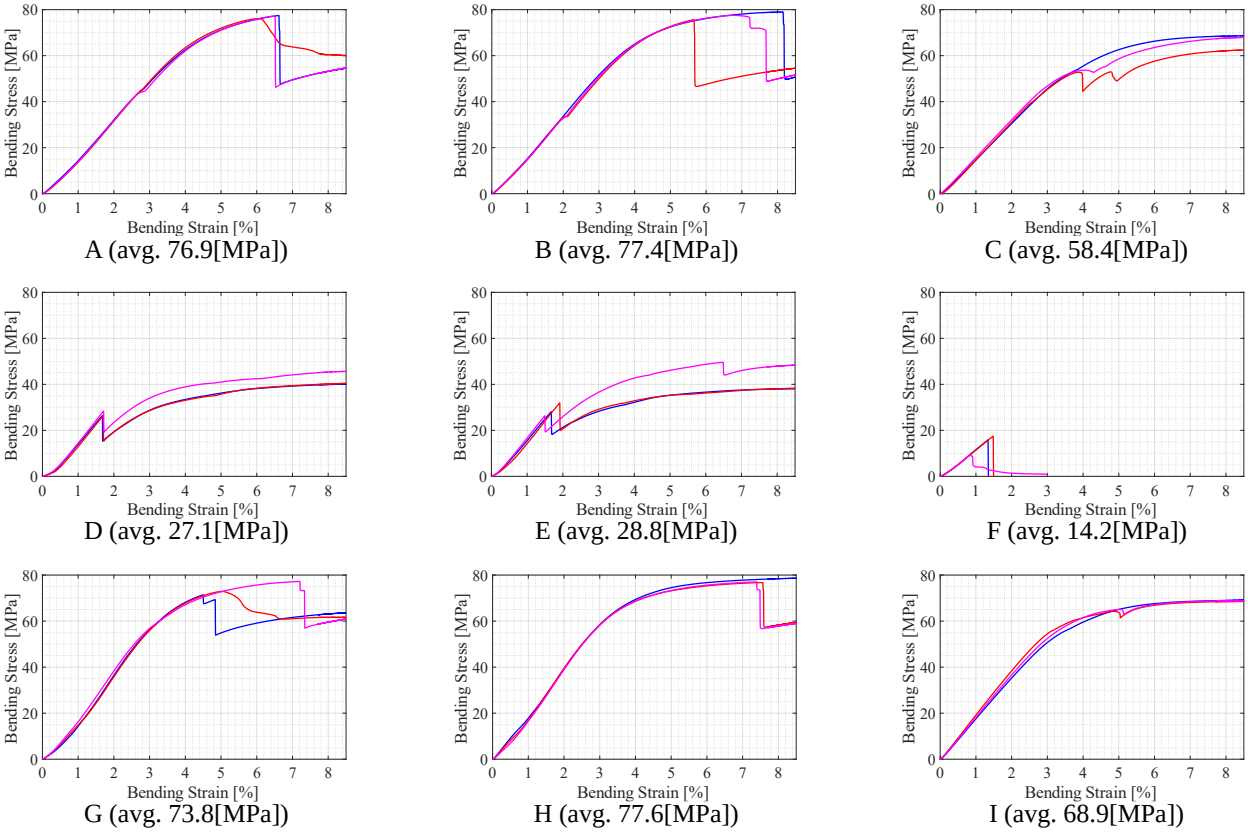

Fig. 7. Experimental results of ABS

TABLE V

SPECIFIC STRENGTH OF SPECIMEN OBTAINED FROM EXPERIMENT

Material	Number	Weight (g)	Specific strength (Nm/g)
POTICON	A	19.4	60.4
POTICON	B	19.6	65.4
POTICON	C	13.6	135.8
POTICON	D	19.8	29.3
POTICON	E	19.9	29.0
POTICON	F	14.3	33.7
POTICON	G	14.9	44.8
POTICON	H	15.0	48.5
POTICON	I	9.5	144.2
ABS	A	16.4	82.3
ABS	B	16.4	83.6
ABS	C	10.6	62.0
ABS	D	17.2	28.4
ABS	E	17.2	30.3
ABS	F	11.1	15.2
ABS	G	12.6	80.7
ABS	H	12.7	85.4
ABS	I	6.9	73.1

taken as the value at the moment the specimen fractured: an avg. 27.1 MPa.

To compare the strength of the specimens with and without embedded pipes, A-C, D-F, and G-I were compared respectively. Considering the averages of the specimens where the pipes were inserted or adhered, in the case of POTICON, A and B were about 0.8 times the value of C, D and E were about 1.4 times the value of F, and G and H were about 0.7 times the value of I. In the case of ABS, A and B were about 1.3 times the value of C, D and E were about 2.0 times the value of F, and G and H were about 1.1 times the value of I. These experimental values differ from those calculated in TABLE IV. Especially, the strength of POTICON specimens was reduced in some cases. The strength of ABS specimens increased, although not as much as compared with TABLE IV. Moreover, it was found that a significant increase in strength, on the order of several tens of times, could not be expected as in the TABLE III comparison.

B. Specific Strength

The experimental specific strengths shown in TABLE V are based on the maximum stresses shown in Fig. 6, 7. In the case of POTICON, the values were larger without the embedded pipe, while in the case of ABS, the opposite was true. Although the pipe is relatively heavy at approximately 7.6 g and the mass of the specimen in which it is embedded is also large, the specific strength of ABS is considered to have been increased due to the sufficient increase in strength.

V. DISCUSSION

A. Observations About Fractures

The test results showed that the addition of the pipe effective by a factor of 0.7 to 2.0, well below the expected factor of several tens of times. One possible reason for this is that the thickness of the resin is thinner in specimens with a pipe, causing a stress concentration at the point where the indenter presses it. Fig. 8 shows the specimens after they

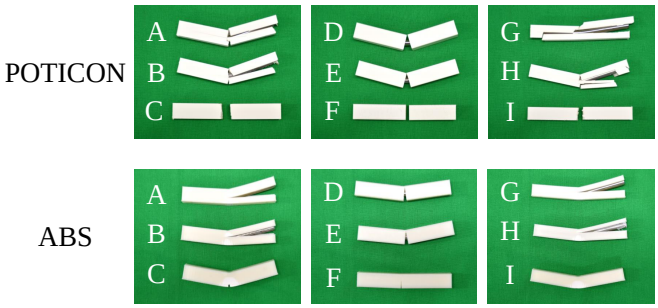

Fig. 8. Fracture specimens

fractured. POTICON in particular is a highly brittle material, and it is thought that the resin portion of the specimen fractured before the pipe was loaded and bent. In fact, at the moment the specimen fractured, shards of resin were observed flying away from the fulcrum with large force. On the other hand, since ABS is a relatively ductile material, the specimen bent and the load was distributed to the pipe, resulting in a larger increase in strength than POTICON. In this case, the specimens fractured cleanly on the fulcrum.

It should be noted that, specimens C and I – laminated in the Z direction and lacking embedded pipes – , bent slowly and eventually formed fractures, whereas some of the specimens with embedded pipes fractured instantaneously. Therefore, it is thought that the reduced wall thickness was the primary cause of fracturing.

B. Difference in Resin Density

The density of the resin portion of each specimen, based on the measured mass and volume, was 92-96% for POTICON and 78-80% for ABS. The reason for the lower density of ABS is thought to be due to the lower filament flow rate setting to prevent resin overflow and unevenness during fabrication of specimens.

C. Analysis of Specimen Properties

The specimen properties are discussed below.

- The lamination direction was compared between specimens A-C and D-F. The results show that the strength of specimens laminated in the Z direction is greater than that of those laminated in the X direction. Since the 3D printed part is anisotropic and the layers tend to peel off in the lamination direction, it is reasonable that the strength of specimens laminated in the Z direction, which is stacked in the direction perpendicular to the load, is greater than those laminated in the X direction.
- Comparing specimens A-C and G-I, in case of no pipe, it was found that specimens with a wall thickness of 2.4 mm had greater strength. The maximum load obtained in the bending test was greater for the specimen with a wall thickness of 3.6 mm, but the experimental stress (strength) for the specimen with a wall thickness of 3.6 mm was superior because of its greater cross-sectional secondary moment.

On the other hand, in the case with pipes, the strength of POTICON specimens with 3.6 mm wall were greater. The difference in strength between the two wall thicknesses was slight for ABS, and some specimens with a wall thickness of 2.4 mm had greater strength.The resin portion of 2.4 mm is thin and easily cracked, but ABS is more ductile than POTICON, so the thin-walled specimens bend more easily and deform together with the pipe, thus showing the greater effect of the pipe.

- Whether the pipe is adhered or not can be compared between specimens A and B, C and D, and G and H. The strength was greater when the pipe was adhered than when it was pressed in, however the difference is negligible. This may be due to the fact that there is only a small gap between the pipe and the specimen, and the adhesive did not penetrate sufficiently.

D. Experimental Procedure Limitations

In this test, as shown in TABLE IV, the flexural rigidity of the resin portion alone was high, and was only several times greater at best when a pipe was inserted. It is speculated that, by shortening the short side of the specimen (thereby reducing the area moment of inertia), the flexural rigidity could have approached the calculated values in TABLE III and the effect could have been several tens of times larger insted. However, as discussed in Section V-C, the reduction in the thickness of the resin portion can be a cause of fracturing, so experimental verification is necessary for specimens with smaller dimensions.

In addition, the pipe is placed in the neutral axis of the specimen in this test, but the stress is greater in the upper and lower portions of the specimen.Therefore, there is a possibility that the strength can be improved by shifting the pipe from the neutral axis and placing it in a position where the stress is greater.

In this paper, only bending tests were conducted to evaluate the strength. Therefore, it can only be said that the embedded pipe method is effective against bending. However, different results may be obtained from tensile or compression tests. Creep tests should also be considered, as they may be effective in reducing creep deformation.

VI. CONCLUSION

In this paper, we hypothesized that embedding a thin-walled metal pipe in a 3D printed beam fabricated by a 3D printer would increase the strength of the part, and conducted a verification test to confirm the effectiveness. Specimens were fabricated from POTICON (a potassium titanate fiber-reinforced material) and ABS resin and subjected to three-point bending tests. As a result, POTICON specimens embedded with stainless steel pipes showed a strength 0.7 to 1.4 times that of the solid specimens, while ABS specimens showed a strength 1.1 to 2.0 times greater than the solid specimens. These values were small compared to our flexural rigidity calculations, and we concluded that embedding a pipe did not significantly increase the strength.

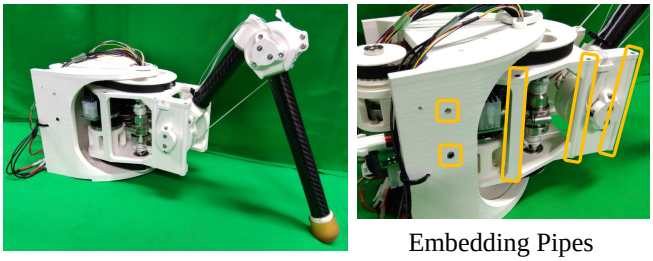

Fig. 9. Application example

As a future prospect, it is possible that the benefit from pipe insertion can be enhanced by reducing the size of the specimen or placing the pipe at the point of high stress in the specimen. In addition to bending, it is also important to conduct tensile, compression, and creep tests to confirm whether the method of embedding thin-walled metal pipes in resin is also effective for these purposes.

We believe that the method proposed in this paper can be applied to reinforcement of robot frames, as shown in Fig. 9. The robot frame is hollow because many parts are placed inside, and it is designed to be strong with columns and walls. However, the wires and timing belts used to move the robot apply large forces to the frame, so thin-walled pipes were placed in these areas to reinforce them. If the method proposed in this paper is effective not only in bending but also in creep deformation, it will be possible to prevent fracture and deformation of the resin and develop robots that are more resistant to breakage.

APPENDIX

The area moment of inertia in Fig. 5 is four times that in the region represented by $y{\geq}0$ and $z{\geq}0$. Therefore, we consider the range of $y{\geq}0$ and $z{\geq}0$. To simplify the calculation, the equivalent area moment of inertia is calculated assuming that all materials are resin. In $r_o{\leq}y{\leq}a$, the material is only resin with flexural modulus E_a, and in $0{\leq}y{\leq}r_o$, the beam is a combination of resin with E_a and a pipe with E_b. In the composite beam, the pipe and the outer resin are in close contact, and the short interval dy of the beam is assumed to be uniaxial tension in the x-axis direction (shear strain in the beam is ignored).

First, the area moment of inertia I_0 at $r_o{\leq}y{\leq}a$ is calculated as follows.

$$I_0 = \int_{r_o}^{a} y^2 dA = \int_{r_o}^{a} y^2 a dy \tag{A.1}$$

Next, $0{\leq}y{\leq}r_o$ is divided into $r_i{\leq}y{\leq}r_o$ and $0{\leq}y{\leq}r_i$.

The vertical force dP_1 at $r_i{\leq}y{\leq}r_o$ is obtained by the following equation.

$$dP_1 = \frac{E_a}{\rho} y b_{a1} dy + \frac{E_b}{\rho} y b_{b1} dy \tag{A.2}$$

where b_{a1} is the Z-axis width of the flexural modulus E_a part, and b_{b1} is that of the E_b part. These can be calculated as follows.

$$b_{b1} = \sqrt{r_o^2 - y^2} \tag{A.3}$$

$$b_{a1} = a - \sqrt{r_o^2 - y^2} \tag{A.4}$$

Similarly to (A.2), the vertical force dP_2 at $0 \leq y \leq r_i$ is as follows.

$$dP_2 = \frac{E_a}{\rho} y b_{a2} dy + \frac{E_b}{\rho} y b_{b2} dy \tag{A.5}$$

where b_{a2} is the Z-axis width of the flexural modulus E_a part, and b_{b2} is that of the E_b part. These can be calculated as follows.

$$b_{b2} = \sqrt{r_o^2 - y^2} - \sqrt{r_i^2 - y^2} \tag{A.6}$$

$$b_{a2} = a - \sqrt{r_o^2 - y^2} \tag{A.7}$$

Using the above, the bending moment M acting on the cross section is calculated using the following equation.

$$M = \frac{E_a}{\rho} I_0 + \int_{r_i}^{r_o} y dP_1 + \int_0^{r_i} y dP_2 = \frac{E_a}{\rho} I' \tag{A.8}$$

Here, the third term of the equation is expressed using the flexural modulus E_a of the resin to derive the equivalent area moment of inertia.

Substituting (A.2)-(A.7) for (A.8), the following equation can be derived.

$$I' = I_0 + \int_{r_i}^{r_o} \left\{ \frac{E_b}{E_a} \sqrt{r_o^2 - y^2} + (a - \sqrt{r_o^2 - y^2}) \right\} y^2 dy + \int_0^{r_i} \left\{ \frac{E_b}{E_a} (\sqrt{r_o^2 - y^2} - \sqrt{r_i^2 - y^2}) + (a - \sqrt{r_o^2 - y^2}) \right\} y^2 dy \tag{A.9}$$

Finally, substitute (A.1) into (A.9) to transform the equation. Calculating $I = 4I'$ yields (1).

ACKNOWLEDGMENT

We thank Otsuka Chemical Co., Ltd. for providing materials and information and for their advice in writing this paper. We thank Prof. Naoyuki Takesue (Tokyo Metropolitan University), and Prof. Yusuke Ohta (Chiba Institute of Techonology), and Prof. Takeshi Takaki (Hiroshima University) for their valuable comments and discussion. We thank Prof. Akira Todoroki (Tokyo Institute of Technology) for his help in deriving Section II-D.

REFERENCES

[1] F. Calignano, D. Manfredi, E. P. Ambrosio, S. Biamino, M. Lombardi, E. Atzeni, A. Salmi, P. Minetola, L. Iuliano, and P. Fino, "Overview on additive manufacturing technologies," *Proceedings of the IEEE*, vol. 105, no. 4, pp. 593–612, 2017.

[2] N. Shahrubudin, T. Lee, and R. Ramlan, "An overview on 3d printing technology: Technological, materials, and applications," *Procedia Manufacturing*, vol. 35, pp. 1286–1296, 2019, the 2nd International Conference on Sustainable Materials Processing and Manufacturing, SMPM 2019, 8-10 March 2019, Sun City, South Africa. [Online]. Available: https://www.sciencedirect.com/science/article/pii/S2351978919308169

[3] Krishnanand, S. Soni, and M. Taufik, "Design and assembly of fused filament fabrication (fff) 3d printers," *Materials Today: Proceedings*, vol. 46, pp. 5233–5241, 2021, international Conference on Innovations in Clean Energy Technologies (ICET2020). [Online]. Available: https://www.sciencedirect.com/science/article/pii/S2214785320365093

[4] W. Roozing and G. Roozing, "3d-printable low-reduction cycloidal gearing for robotics," in *2022 IEEE/RSJ International Conference on Intelligent Robots and Systems (IROS)*, 2022, pp. 1929–1935.

[5] K. Urs, C. E. Adu, E. J. Rouse, and T. Y. Moore, "Design and characterization of 3d printed, open-source actuators for legged locomotion," in *2022 IEEE/RSJ International Conference on Intelligent Robots and Systems (IROS)*, 2022, pp. 1957–1964.

[6] T. Yoshida, G. Endo, A. Okubo, and H. Nabae, "Experimental evaluation of a quasi-direct-drive actuator with a 3d-printed planetary gear reducer," in *2023 IEEE/SICE International Symposium on System Integration (SII)*, 2023, pp. 1–6.

[7] F. Grimminger, A. Meduri, M. Khadiv, J. Viereck, M. Wüthrich, M. Naveau, V. Berenz, S. Heim, F. Widmaier, T. Flayols, J. Fiene, A. Badri-Spröwitz, and L. Righetti, "An open torque-controlled modular robot architecture for legged locomotion research," *IEEE Robotics and Automation Letters*, vol. 5, no. 2, pp. 3650–3657, 2020.

[8] "CRANE-X7," [Online]. Available: https://rt-net.jp/products/crane-x7/. Accessed: Jul. 16, 2023.

[9] M. Lapeyre, P. Rouanet, J. Grizou, S. N'Guyen, A. Le Falher, F. Depraetre, and P.-Y. Oudeyer, "Poppy: Open source 3d printed robot for experiments in developmental robotics," in *4th International Conference on Development and Learning and on Epigenetic Robotics*, 2014, pp. 173–174.

[10] M. Heidari-Rarani, M. Rafiee-Afarani, and A. Zahedi, "Mechanical characterization of fdm 3d printing of continuous carbon fiber reinforced pla composites," *Composites Part B: Engineering*, vol. 175, p. 107147, 2019. [Online]. Available: https://www.sciencedirect.com/science/article/pii/S1359836818335686

[11] N. Li, Y. Li, and S. Liu, "Rapid prototyping of continuous carbon fiber reinforced polylactic acid composites by 3d printing," *Journal of Materials Processing Technology*, vol. 238, pp. 218–225, 2016. [Online]. Available: https://www.sciencedirect.com/science/article/pii/S0924013616302515

[12] M. H. Ali, G. Yerbolat, and S. Amangeldi, "Material optimization method in 3d printing," in *2018 IEEE International Conference on Advanced Manufacturing (ICAM)*, 2018, pp. 365–368.

[13] D. Li, N. Dai, X. Jiang, Z. Shen, and X. Chen, "Density aware internal supporting structure modeling of 3d printed objects," in *2015 International Conference on Virtual Reality and Visualization (ICVRV)*, 2015, pp. 209–215.

[14] Markforged, "Mark Two," [Online]. Available: https://markforged.com/3d-printers/mark-two, Accessed: Aug. 3, 2023.

[15] J. Sudheer Reddy, B. A. Praveena, V. Kedambadi Vasu, N. Lokesh, P. Prabhakar, K. K. Sunil, K. Mohan, and V. Thapa, "Mechanical characterization of graphene reinforced pla composites printed by fused deposition modelling," in *2022 IEEE 2nd Mysore Sub Section International Conference (MysuruCon)*, 2022, pp. 1–6.

[16] F. van der Klift, Y. Koga, A. Todoroki, M. Ueda, Y. Hirano, and R. Matsuzaki, "3d printing of continuous carbon fibre reinforced thermo-plastic (cfrtp) tensile test specimens," *Open Journal of Composite Materials*, vol. 06, pp. 18–27, 01 2016.

[17] A. Kvalsvig, X. Yuan, J. Potgieter, and P. Cao, "3d printing of fibre reinforced honeycomb structured composite materials," in *2016 23rd International Conference on Mechatronics and Machine Vision in Practice (M2VIP)*, 2016, pp. 1–6.

[18] Otsuka Chemical Co., Ltd., "POTICON TISMO Reinforced Compound," [online]. Available: https://www.otsukac.co.jp/en/products/chemical/poticon/, Accessed: Jul. 16, 2023.

[19] Otsuka Chemical Co., Ltd., "Technical data sheet POTICON filament NTL34M," [online]. Available: https://raise3d.jp/wp/wp-content/uploads/2022/06/TDS_JP_POTICON_NTL34M_202230120.pdf, Accessed: Aug. 3, 2023.

[20] Zortrax S.A., "TECHNICAL DATA SHEET Z-ULTRAT," [Online]. Available: https://www.zortrax.sin.jp/_files/ugd/a934e6_43b67683f347481bab6138835f43da1d.pdf, Accessed: Aug. 3, 2023.